European Journal of Medicinal Chemistry 220 (2021) 113436

Contents lists available at ScienceDirect

European Journal of Medicinal Chemistry

journal homepage: http://www.elsevier.com/locate/ejmech

A γ-lactam siderophore antibiotic effective against multidrug-resistant *Pseudomonas aeruginosa*, *Klebsiella pneumoniae*, and *Acinetobacter* spp.

Joel A. Goldberg [a], Vijay Kumar [b], Elizabeth J. Spencer [c], Denton Hoyer [c], Steven H. Marshall [a], Andrea M. Hujer [a, d], Kristine M. Hujer [a, d], Christopher R. Bethel [a], Krisztina M. Papp-Wallace [a, b, d], Federico Perez [a, d, e], Michael R. Jacobs [d, f], David van Duin [g], Barry N. Kreiswirth [h], Focco van den Akker [b, **], Mark S. Plummer [c, ***], Robert A. Bonomo [a, b, d, e, i, j, *]

[a] *Research Service, Louis Stokes Cleveland Department of Veterans Affairs Medical Center, Cleveland, OH, 44106, USA*
[b] *Department of Biochemistry, Case Western Reserve University, Cleveland, OH, 44106, USA*
[c] *Yale Center for Molecular Discovery, West Haven, CT, 06516, USA*
[d] *Department of Medicine, Case Western Reserve University, Cleveland, OH, 44106, USA*
[e] *Geriatric Research, Education and Clinical Center, Louis Stokes Cleveland Department of Veterans Affairs Medical Center, Cleveland, OH, 44106, USA*
[f] *Department of Pathology, University Hospitals Cleveland Medical Center, Division of Clinical Microbiology, Cleveland, OH, 44106, USA*
[g] *University of North Carolina School of Medicine, Chapel Hill, NC, 27514, USA*
[h] *Center for Discovery and Innovation, Hackensack Meridian Health, Nutley, NJ, 07601, USA*
[i] *Departments of Pharmacology, Molecular Biology & Microbiology, And Proteomics & Bioinformatics, Case Western Reserve University, Cleveland, OH, 44106, USA*
[j] *CWRU-Cleveland VAMC Center for Antimicrobial Resistance and Epidemiology (Case VA CARES), Cleveland, OH, 44106, USA*

ARTICLE INFO

Article history:
Received 4 February 2021
Received in revised form
23 March 2021
Accepted 30 March 2021
Available online 8 April 2021

Keywords:
γ-Lactam
Siderophore
Multidrug-resistant gram-negative pathogens
Penicillin-binding protein

ABSTRACT

Serious infections caused by multidrug-resistant (MDR) organisms (*Klebsiella pneumoniae*, *Pseudomonas aeruginosa*, *Acinetobacter baumannii*) present a critical need for innovative drug development. Herein, we describe the preclinical evaluation of YU253911, **2**, a novel γ-lactam siderophore antibiotic with potent antimicrobial activity against MDR Gram-negative pathogens. Penicillin-binding protein (PBP) 3 was shown to be a target of **2** using a binding assay with purified *P. aeruginosa* PBP3. The specific binding interactions with *P. aeruginosa* were further characterized with a high-resolution (2.0 Å) X-ray structure of the compound's acylation product in *P. aeruginosa* PBP3. Compound **2** was shown to have a concentration >1 μg/ml at the 6 h time point when administered intravenously or subcutaneously in mice. Employing a meropenem resistant strain of *P. aeruginosa*, **2** was shown to have dose-dependent efficacy at 50 and 100 mg/kg q6h dosing in a mouse thigh infection model. Lastly, we showed that a novel γ-lactam and β-lactamase inhibitor (BLI) combination can effectively lower minimum inhibitory concentrations (MICs) against carbapenem resistant *Acinetobacter* spp. that demonstrated decreased susceptibility to **2** alone.

Abbreviations: MDR, multidrug-resistant; PBP, penicillin-binding protein; MIC, minimal inhibitory concentration; *blas*, β-lactamases; SC, subcutaneously; IM, intramuscularly; CFU, colony-forming unit; WGS, whole-genome sequencing; CRAB, carbapenem-resistant *Acinetobacter baumannii*; CSAB, carbapenem-susceptible *Acinetobacter baumannii*; BLIs, β-lactamase inhibitors; LCMS, liquid chromatography mass spectrometry; NMR, nuclear magnetic resonance; UV, ultraviolet; DMSO, dimethylsulfoxide; MSTFA, *N*-methyl-*N*-(trimethylsilyl)-trifluoroacetamide; AN, *Acinetobacter nosocomialis*; FI, fluorescence intensity; SAR, structure activity relationship.

* Corresponding author. Research Service, Louis Stokes Cleveland Department of Veterans Affairs Medical Center, Cleveland, OH, 44106, USA.
** Corresponding author.
*** Corresponding author.
E-mail addresses: fxv5@case.edu (F. van den Akker), marksplummer@gmail.com (M.S. Plummer), Robert.Bonomo@va.gov (R.A. Bonomo).

https://doi.org/10.1016/j.ejmech.2021.113436
0223-5234/

1. Introduction

Multidrug-resistant (MDR) bacterial infections pose an increasing threat to public health, causing significant morbidity, mortality, and economic hardship. In the United States alone, more than three million infections each year are caused by antibiotic-resistant bacteria resulting in approximately 36,000 deaths and more than $20 billion in healthcare costs [1]. The future global impact is even more staggering with an estimated cumulative economic cost of $100 trillion from now until 2050, with an associated 10 million deaths, resulting from MDR infections [2]. Invasive infections with Gram-negative bacterial pathogens in particular have become increasingly problematic and are associated with 28 day mortality rates of 30–70% (https://www.cdc.gov/drugresistance/biggest-threats.html). Resistant strains of *Acinetobacter baumannii*, *Pseudomonas aeruginosa*, and carbapenem-resistant Enterobacterales are identified as "urgent" and "serious" threats by the CDC and WHO, illustrating the critical need for new therapeutics [3–7].

The "hard-to-treat" nature of these infections is often caused by extensive antibiotic-resistant phenotypes that allow pathogens to overcome standard antibiotic regimens [8]. Despite the increasing public health threat, few truly novel agents are in development to treat such infections, as most large pharmaceutical companies have withdrawn from antibacterial research [3,4,9,10]. Government agencies are aware of the ever-growing issue of antibacterial resistance and are responding with several initiatives intended to incentivize renewed efforts in antibiotic development [11]. They include public-private partnerships highlighting the urgent need for novel treatments.

Resistance in multidrug-resistant Gram-negative organisms is multifactorial. These causes may include reduced permeability, modification of target proteins, and overexpression of efficient and diverse efflux pumps [12,13]. For β-lactam antibiotics, a particular concern is the increasing diversity of plasmid-mediated carbapenemases (β-lactamases (*blas*): NDM-1, KPC, and OXA-type class D carbapenemases) making β-lactam antibiotics ineffective, despite their common coadministration with β-lactamase inhibitors [1].

We recently reported the initial attributes of an antibacterial agent effective against Gram-negative pathogens based on a revitalized non-β-lactam pyrazolidinone scaffold [14–21] exemplified by **1** (Fig. 1) [22]. The strategy involves inhibiting penicillin-binding proteins (PBPs), which are validated targets for antibacterial discovery, while avoiding susceptibility to β-lactamase inactivation. This is accomplished by using a γ-lactam ring with tunable reactivity as the molecule's core [18,20]. Additionally, **1** includes a siderophore moiety which exploits intrinsic bacterial iron transport processes ("Trojan horse approach") to overcome the decreased permeability of Gram-negative bacteria [23–25]. Agent **1**, which contains a prototype γ-lactam-siderophore, inactivates PBP3 and possesses excellent *in vitro* potency against MDR clinical isolates of *P. aeruginosa*, *K. pneumoniae*, and *E. coli*. Herein, we report the discovery and properties of YU253911, **2**, a chloroaminothiazole analog of **1** (Fig. 1), which possesses enhanced potency versus *Acinetobacter* spp. and improved pharmacokinetics versus **1** as illustrated by *in vivo* efficacy in a rodent thigh infection model employing an MDR strain of *P. aeruginosa*.

2. Results and discussion

2.1. Chemistry

We previously reported the synthesis and characterization of **1** as a prototype of a new class of siderophore-conjugated γ-lactam antibiotic with enhanced activity against MDR Gram-negative bacteria [22]. In an effort to explore this finding, additional analogs with modified side chains were screened, leading to the identification of **2** which contains a chloroaminothiazole group. This group was found to favorably modulate several biological properties (*vide infra*). The synthesis of **2** parallels the synthesis of **1** and employs a common advanced intermediate dihydroxyphthalimide [26] -appended bicyclic pyrazolidinone, **14** (details of the synthesis of **14** are in the Supporting Information, pages 4–17). Coupling of **14** using the appropriately protected chloroaminothiazole **15** followed by deprotection and reverse phase chromatography provides compound **2**, Scheme 1. The chiral purity of **2** was not assessed after the synthesis was completed though Boc-L-serine was employed as the starting material.

2.2. Microbiology

2.2.1. γ-Lactam 2 inhibits the growth of MDR Gram-negative bacilli

A comparison of minimum inhibitory concentrations (MICs) for **2** and **1** vs. previously described clinical carbapenem-resistant isolates of *P. aeruginosa* [27] and *K. pneumoniae* [28] are provided in Fig. 2 [22]. MIC data for both **2** and **1** is provided for comparison; the detailed values for each individual strain are in Supplemental Table 1, page 18. In all but one case (YUKP-39), microbiologic potency of **2** was maintained, although the activity trended to be slightly less active for **2** compared to **1**, particularly for *K. pneumoniae*. Nevertheless, MIC testing of **2** afforded an MIC_{50} of 0.5 and 1 μg/mL against 23 samples each of MDR *P. aeruginosa* and *K. pneumoniae*, respectively. Notably, MIC data of **2** were significantly lower than meropenem in all cases but 1 isolate (YUKP-39). We purposely selected a subset of our *P. aeruginosa* and *K. pneumoniae* panels that had the most potent compound **1** MIC values. Using such a narrow comparison means it is possible that **2** may not necessarily have poorer overall activity against larger panels. Similar to what was previously reported for **1** [22], MIC values were dependent on maintaining low iron concentrations in the culture media (data not shown). All results were generated using Chelex® resin-treated media to mimic the low iron concentrations found *in vivo*, and in accord with CLSI recommendations for siderophore-containing antibiotics.

2.2.2. The γ-lactam 2 possesses enhanced antimicrobial activity against MDR A. baumannii

MICs in low iron media against a 198-member panel of previously described *Acinetobacter* spp. clinical isolates, (79% *A. baumannii*, 21% a mixture of *A. nosocomialis*, and *A. pittii*) [30] are presented in Fig. 3 and Table 1. Activity against a 98-member carbapenem-resistant *A. baumannii* subset of the panel is also shown in Fig. 3 and Table 1. Importantly, the MIC values of **2** compare favorably to all β-lactam classes, including aztreonam **3** (monobactam), ceftazidime **4** (cephalosporin) and meropenem **5** (carbapenem) (Table 1). Applying the breakpoints for cefiderocol **9** (susceptibility $\leq$4 μg/mL and resistance $\geq$16 μg/mL), a similar approved drug utilizing a siderophore transport mechanism [29], to compound **2** results in a susceptibility to **2** of 86% (171 out of 198) of the full *Acinetobacter* panel and 83% (81 out of 98) of the subset of carbapenem-resistant *A. baumannii* (CRAB). Detailed values for each individual strain are in Supplemental Table 2, page 19.

2.2.3. Combination of 2 with sulbactam further enhances growth inhibition of Acinetobacter spp.

We investigated whether partner agents could improve the already potent activity of **2** against resistant *Acinetobacter* spp. growth. β-lactam antibiotics are often used clinically in combination with β-lactamase inhibitors (BLIs) to protect against enzymatic hydrolysis. Although the γ-lactam core of **2** possesses intrinsic

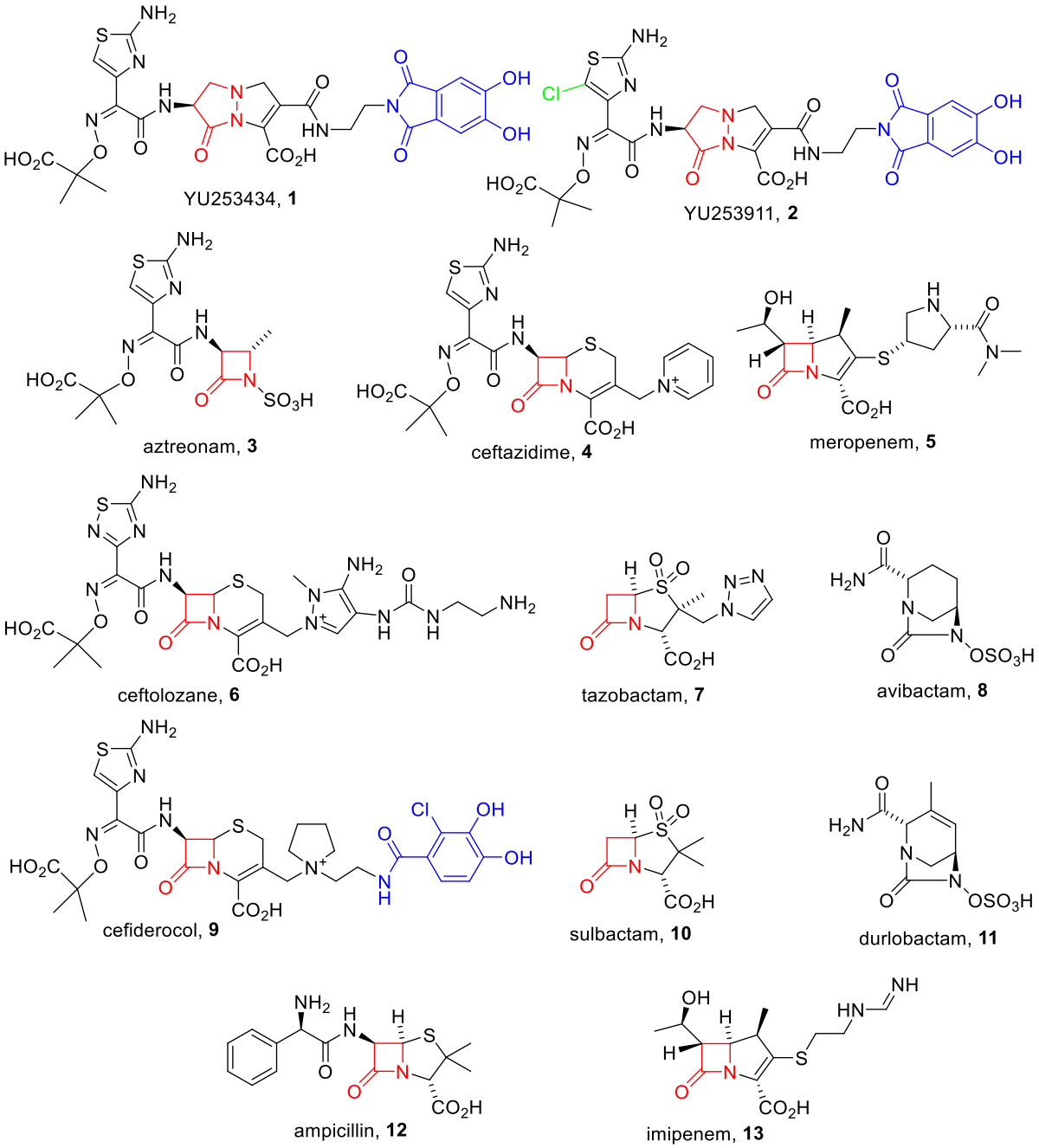

Fig. 1. Structures of γ-lactam siderophores **1** and **2** versus comparator β-lactam antibiotics and β-lactamase inhibitors. The β- or γ-lactam core is highlighted in red; iron-binding siderophore moieties in blue.

stability to β-lactamase hydrolysis (*vide infra*), β-lactamase inhibitors (BLIs) were nevertheless evaluated for their ability to augment the breadth of **2** effectiveness against *Acinetobacter* spp.

Sulbactam **10**, a BLI commonly marketed in combination with ampicillin (**12**, Unasyn®), was selected for study as a potential partner of **2** for two reasons. Firstly, sulbactam has been shown for decades to be safe [31,32] and well-tolerated in patients [33], with favorable pharmacokinetics [34,35]; secondly, sulbactam possesses intrinsic antimicrobial activity against *Acinetobacter* spp. due to postulated inhibition of PBP1 and PBP3 [36]. Furthermore, sulbactam is currently under investigation in combination with durlobactam, **11**, for the treatment of *Acinetobacter* infections. The γ-lactam **2** is believed to target PBP3 (*vide infra*) and inhibition of two PBP enzymes would be expected to produce enhanced antimicrobial effects.

The 24 *Acinetobacter* isolates from Fig. 3 with higher MICs to compound **2** (MIC≥16 μg/mL) were tested versus sulbactam alone or in combination with **2**. MIC values show 79% (19/24) of the tested isolates were found to have their growth inhibited to some extent by sulbactam (MICs≤16 μg/mL) (Table 2). Furthermore, when **2** and sulbactam were combined in a 1:1 ratio in a typical 2-fold MIC dilution scheme, 50% (12/24) of the isolates previously resistant to **2** showed improved MICs≤4 μg/mL. Published human pharmacologic data for ampicillin-sulbactam and sulbactam-durlobactam

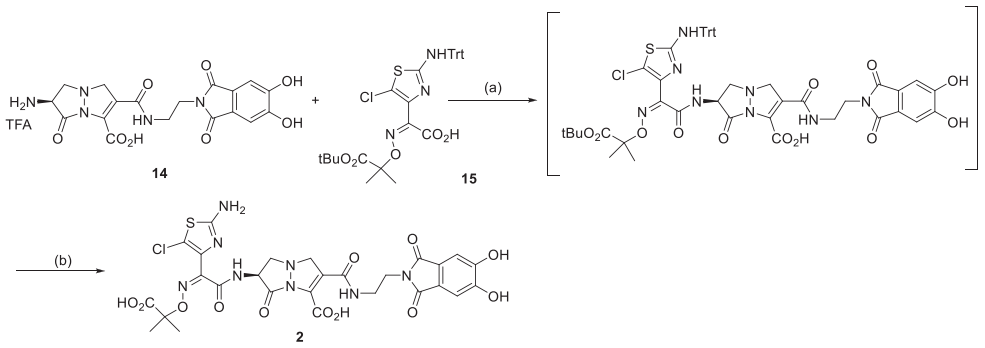

Scheme 1. Synthesis of YU253911, **2**: (a) i. **15**, Oxalyl chloride, catalytic DMF; ii) **14**, MSTFA, Hunig's base, 3.5 h, 100% crude. (b) 2:1 DCM/TFA, triethylsilane, 0 °C to RT, 1.5 h, toluene chase, reverse phase MPLC C18, 0–60% acetonitrile 0.1% formic acid/water with 0.1% formic acid, 30%.

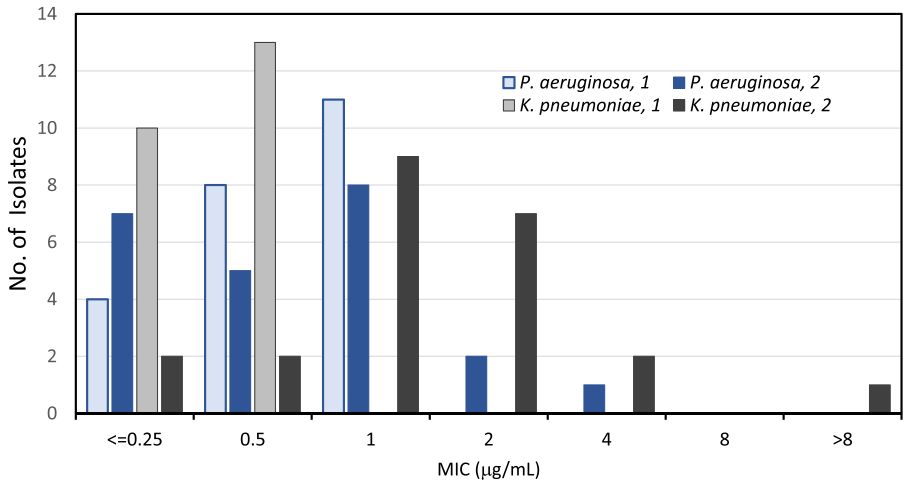

Fig. 2. Compound **2** and **1** MIC values against representative γ-lactam susceptible/carbapenem-resistant *K. pneumoniae* and *P. aeruginosa* strains (23 each). Except for one isolate, YUKP-39, compound **2** maintains microbiologic potency against MDR Gram-negative rods previously described for this γ-lactam-siderophore class (see also Supplemental Table 1, page 18).

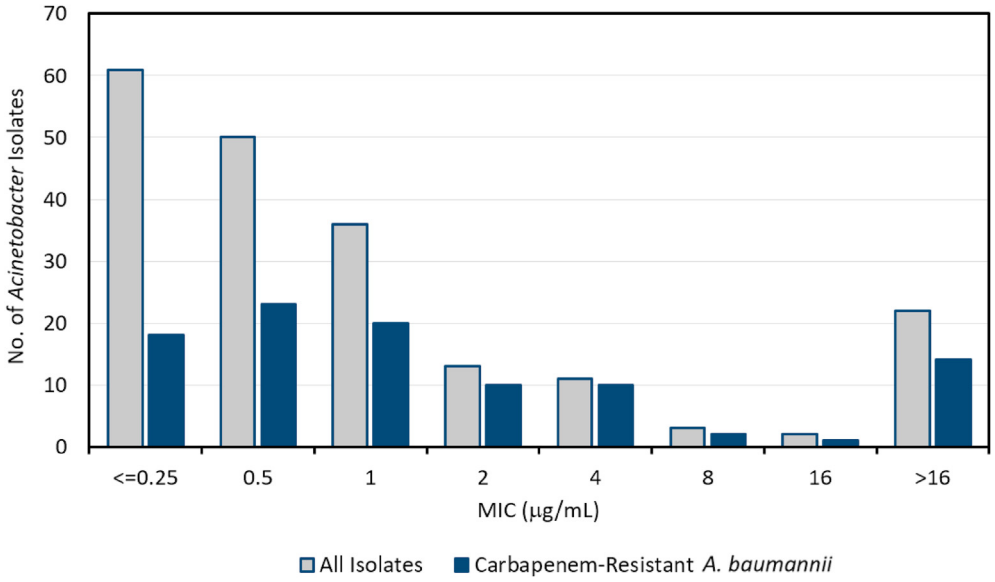

Fig. 3. Distribution of MICs in low iron media of **2** (μg/mL) against a 198-member *Acinetobacter* spp. panel and subset of 98 carbapenem-resistant *A. baumannii* (CRAB) isolates. See also Supplemental Table 2, page 19.

Table 1
MIC_{50} and MIC_{90} (μg/mL) of **2** and comparator β-lactam antibiotics against a 198-member panel of clinical isolates of *Acinetobacter* spp., as well as the 98-member subset of carbapenem-resistant *A. baumannii* (CRAB).[30] Chemical structures for all agents are provided in Fig. 1.[a] See also Supplemental Table 2, page 19.

Compound	198 *Acinetobacter* spp.		98 CRAB	
	MIC_{50}	MIC_{90}	MIC_{50}	MIC_{90}
2	0.5	>16	1	>16
Aztreonam (**3**)	>32	>32	>32	>32
Ceftazidime (**4**)	64	>64	>64	>64
Meropenem (**5**)	8	>64	64	>64
Ceftazidime (**4**)/avibactam (**8**)	16	>64	64	>64
Ceftolozane (**6**)/tazobactam (**7**)	8	>64	32	>64

[a] MICs were determined using iron-depleted cation-adjusted Mueller-Hinton broth that was supplemented with iron (as ferric chloride) as indicated. The initial iron-depleted media was prepared by the standard treatment with cation-exchange resin, which has been reported to reduce iron concentrations to 0.02 μg/mL[29].

demonstrate that serum concentrations of sulbactam of 20 μg/mL are readily attainable from intravenous dosing. Therefore, additional studies were undertaken to evaluate the *in vitro* effectiveness of **2** under conditions of a constant level of sulbactam coadministration. The MIC values for **2** were determined using sulbactam set at 20 μg/mL (Table 2). Under these conditions, the growth of only 3 of the isolates resistant to **2** were not significantly inhibited, collectively implying that 98% of the full 198 member *Acinetobacter* spp. panel could be susceptible to **2** when used in combination with a 20 μg/mL coadministration of sulbactam.

2.3. PBP inhibition

Based on the mechanism established previously for γ-lactam **1**, **2** was also suspected of inhibiting PBP3, an essential bacterial transpeptidase. This was verified through labeling studies with Bocillin™, a fluorescent penicillin analog, using purified *P. aeruginosa* PBP3 according to an established protocol [37]. Increasing concentrations of **2** inhibited fluorescent labeling of the protein by Bocillin™, with an IC_{50} of 5 ± 1 μM (Fig. 4). This value is comparable to **1** (2.5 ± 0.5 μM) and a previously published value for doripenem (IC_{50} = 2.3 ± 0.5 μM, for *Acinetobacter* spp. PBP3) [37].

Table 2
MIC (μg/mL) values in low iron media of **2** in combination with sulbactam, **10**, when combined 1:1 (by mass), or when **2** was tested with a constant concentration of **10** at 20 μg/mL. Individual MIC values for **2** and **10** are provided for comparison as well as the identity of each *Acinetobacter* isolate. See text for details.

Isolate No	Strain Identity[a]	2	10	2 + 10 (1:1)	2 + 10 (20 μg/mL)
PR-314	CRAB	>16	16	4	≤0.25
PR-319	CRAB	>16	>32	4	0.5
PR-325	CRAB	>16	32	>16	>16
PR-326	CRAB	>16	2	2	≤0.25
PR-340	CSAB	>16	4	1	≤0.25
PR-342	CRAB	16	>32	>16	>16
PR-345	CRAB	>16	16	16	≤0.25
PR-351	CRAB	>16	16	16	≤0.25
PR-362	AN	>16	1	≤0.25	≤0.25
PR-365	AN	>16	1	≤0.25	≤0.25
PR-380	CRAB	>16	16	16	≤0.25
PR-384	CRAB	>16	16	16	>16
PR-387	CRAB	>16	16	16	≤0.25
PR-399	CRAB	>16	16	16	≤0.25
PR-401	CRAB	>16	16	8	≤0.25
PR-412	AN	>16	2	1	≤0.25
PR-423	CRAB	>16	16	8	≤0.25
PR-434	CSAB	>16	8	2	≤0.25
PR-452	CSAB	>16	1	≤0.25	≤0.25
PR-459	CRAB	16	32	8	4
PR-464	CSAB	>16	1	≤0.25	≤0.25
PR-478	CSAB	16	4	1	≤0.25
PR-482	CRAB	>16	32	>16	≤0.25
PR-491	AN	>16	2	0.5	≤0.25

[a] Strain identity: CRAB = carbapenem-resistant *A. baumannii*; CSAB = carbapenem-susceptible *A. baumannii*; AN = *A. nosocomialis* (carbapenem-susceptible).

2.4. The compound 2 crystal structure complexed with P. aeruginosa PBP3a

The crystal structure of *P. aeruginosa* PBP3 complexed to **2** was determined to 2.0 Å resolution (Table 3). The difference electron density in the active site shows that **2** has formed a covalent bond with the catalytic S294 residue (Fig. 5). Density for most of the compound **2** moieties is well resolved. This includes the chlorine substituent on the aminothiazole ring, both amide groups, the carboxyl group and the dihydropyrazole ring of the core. Note that the occupancy for the chlorine atom refined to 0.58 whereas the rest of the aminothiazole ring had an occupancy of 1.0. This decreased occupancy for the chlorine atom is likely due to radiation damage during the synchrotron radiation X-ray experiment. Halogen-aromatic ring bonds are known to be sensitive to X-ray radiation, and their breakage has been used to monitor radiation damage in protein crystals [38]. Density for the 2-carboxypropan-dimethyl moiety extending from the oxime and the 5,6-dihydroxyphthalimide siderophore group of **2** are not well resolved in the electron density map indicating their inherent flexibility (Fig. 5).

The ligand **2** forms a number of hydrogen bonds in the active site of *P. aeruginosa* PBP3 (Fig. 6). The chloroaminothiazole ring hydrogen bonds with E291, and main chain oxygen and nitrogen atoms of R489. The chloroaminothiazole also makes hydrophobic interactions with G293, Y409, and A488. In addition, the chlorine substituent makes a special close-to-linear "C-Cl ⋯ O″ interaction with the carbonyl oxygen of Y407. Such favorable interactions with a halogen atom have previously been observed in protein:ligand interactions [39,40]. The amide side chain, which connects to the aminothiazole ring, hydrogen bonds with N351 and the backbone oxygen of T487. The carboxyl moiety of the core hydrogen bonds with T487, S485, and conformation 2 of residue S349. The secondary nitrogen atom of the dihydropyrazole ring hydrogen bonds with conformation 1 of S349 (Fig. 6). The amide moiety that serves to attach the 5,6-dihydroxyphthalimide siderophore side chain of **2** interacts with a nearby water molecule (W#2). The 5,6-dihydroxyphthalimide does not form many interactions in the active site.

The compound **2** is chemically identical to the previously reported **1,** except the 5-position of the aminothiazole in **2** has a chloro-substituent. The binding mode of **1** is very similar to that of **2** when bound to *P. aeruginosa* PBP3 (Fig. 7; PDBid 6VOT) [22]. A difference is an inversion of the tertiary nitrogen in the dihydropyrazole ring of **2** compared to **1**. This is likely a consequence of that the **2 PBP3** complex is determined to a higher resolution (2.0 vs. 2.5 Å resolution) allowing for improved refinement of this ring region. A second difference is that residue E291 in the **2 PBP3** complex has moved closer to the aminothiazole ring compared to the **1 PBP3** complex (Fig. 7).

2.5. Pharmacokinetics and in vivo efficacy; drug-like attributes

Pyrazolidinone **2** has many characteristics that are favorable drug-like attributes (details of the data are found in the Supporting Information, pages 33–38) for potential administration either by IV or inhaled routes as **2** has high solubility >100 μM in pH 7.5 phosphate buffer as measured by nephelometry. Though highly

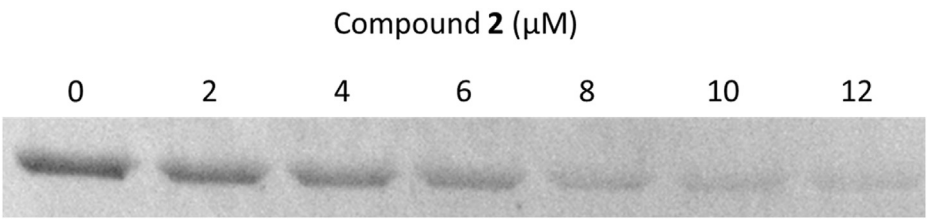

Fig. 4. Determination of the IC_{50} of **2** for *P. aeruginosa* PBP3 using a competitive assay. Bocillin™, a fluorescent substrate of PBP3 was reacted with enzyme that had been pre-incubated with increasing concentrations of **2**. An IC_{50} was calculated as the concentration of **2** required to reduce the fluorescence intensity of the Bocillin™-labeled protein by 50%.

Table 3
X-ray diffraction data collection and crystallographic refinement statistics for the *P. aeruginosa* PBP3 complex with **2**.

Wavelength (Å)	0.97946
Resolution range (Å)	50.00–2.00 (2.03–2.00)
Space group	$P2_12_12_1$
Unit cell (Å, °)	67.77 82.66 88.80 90 90 90
Total reflections	427,156
Unique reflections	34,157 (1,673)
Multiplicity	12.5 (12.6)
Completeness (%)	99.8 (99.8)
Mean I/sigma (I)	30.5 (4.4)
$CC_{1/2}$	0.995 (0.934)
R-merge (%)	15.8 (115.9)
Resolution refinement (Å)	33.91–2.00 (2.05–2.00)
Reflections used in refinement	32,335 (2,169)
Reflections used for R-free	1,770 (141)
R-work	0.174 (0.202)
R-free	0.227 (0.237)
Number of non-hydrogen atoms	3,863
Macromolecules	3,621
Ligand	49
Solvent	193
Protein residues	473
RMS(bonds, Å)	0.010
RMS(angles, °)	1.65
Ramachandran favored (%)	97.64
Ramachandran allowed (%)	2.15
Ramachandran outliers (%)	0.22

Statistics for the highest-resolution shell are shown in parentheses.

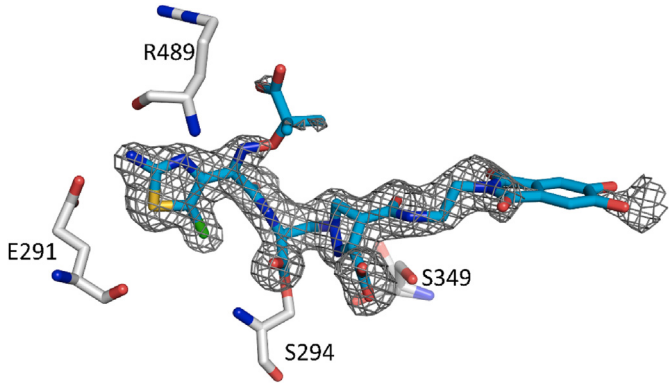

Fig. 5. Omit Fo-Fc electron density showing the presence of a covalently bound **2**. The compound **2** is shown with cyan-colored carbon atoms. The density is contoured at the 3 σ level.

soluble, **2** has poor Caco-2 permeability and would not be expected to have oral bioavailability thus IV and sub cutaneous PK was obtained (*vide infra*). Compound **2** is highly protein-bound as shown by measurements in both mouse and human plasma, 94% and 88%, respectively. Stability of **2** to both human and CD-1 mouse microsomes is notable with a half-life >60 min in both preparations. Furthermore, **2** does not inhibit 7 of the 8 CYP enzymes it was tested against at a 30 μM concentration and showed approximately 50% inhibition of CYP2C8 at 100 μM. Compound **2** was also evaluated for cytotoxicity was not found when tested against human primary hepatocytes at a maximal dose of 100 μM.

In a general safety screen, testing **2** against 44 enzymes and receptors the only activity of note was >50% inhibition at 30 μM against cyclooxygenase (COX-1) and phosphodiesterase PDE3A (Supporting Information, page 37). Testing against 6 ion channels, including hERG at a 30 μM maximal dose revealed **2** did not inhibit these channels (Supporting Information, page 38). The pharmacokinetics (PK) of **2** was evaluated both subcutaneously and by intravenous administration at a dose of 50 mg/kg in CD-1 mice (Table 4). Both routes of dosing result in similar PK data. Notably, the plasma levels of **2**, at the 6h time point were >1.0 μg/mL by both dosing routes (Fig. 8 and Table 4). This value is clearly superior to **1** where at the 6-h timepoint its plasma concentration was about 0.35 μg/mL [22]. The cause for improved plasma level with **2** is not known, though it might be due to clearance differences caused by a slight increase in protein binding or a small increase in LogP due to the additional chlorine atom. Nevertheless, the >1.0 μg/mL plasma level encouraged us to comparatively test both **2** and **1** in a mouse efficacy model as this plasma level is above the MIC_{50} values of **2** for both *P. aeruginosa* and *A. baumannii*.

We chose AR-BANK#0229 strain of carbapenem-resistant *P. aeruginosa* as the infectious agent for the neutropenic thigh infection model. This decision was made for several reasons: a) this strain establishes infection in mice; b) both compound **2**, and **1** have potent activity against this strain (MIC = 0.5 μg/ml and 0.25 μg/mL, respectively); and c) the strain is highly resistant to currently clinically used antibiotics as it is susceptible to only colistin, amikacin, and gentamicin (Supplemental Table 4, page 42).

Neutropenia was induced with cyclophosphamide. Animals were then intramuscularly (IM) inoculated with 1.02×10^6 CFU/mouse (0.1 mL/animal) of the *P. aeruginosa* AR-BANK#0229 strain. Test antibiotics, **1** and **2**, both at 50 and 100 mg/kg, were administered subcutaneously (SC) four times per day (QID) with 6 h intervals (q6h) at 2, 8, 14 and 20 h after infection. The reference control was colistin, which was dosed at 30 mg/kg and administered subcutaneously (SC) twice (BID) with 12 h intervals (q12h) at 2 and 14 h after infection. Animals were sacrificed at 2 or 26 h post-infection, and the thigh tissues were harvested and weighed from each of the test animals. The bacterial counts (CFU/g) of thigh tissue homogenates were compared. Full details of the method and protocol are in the Supplemental Information as well as the individual animal data (Supplemental Information, pages 45–57). Bacterial burden (CFU/g tissue) of test article treated animal groups was compared to the baseline bacterial count at 2 h after infection and the difference in counts (Δ) was reported. The significance of effects was assessed with ANOVA. The burden was also compared to the vehicle control.

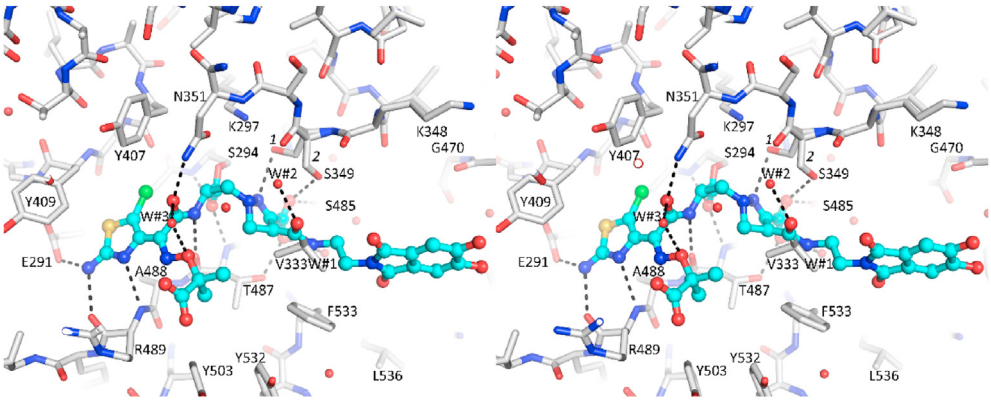

Fig. 6. Stereo diagram depicting the interactions of **2** in the active site of *P. aeruginosa* PBP3. Hydrogen bonds are depicted as dashed lines.

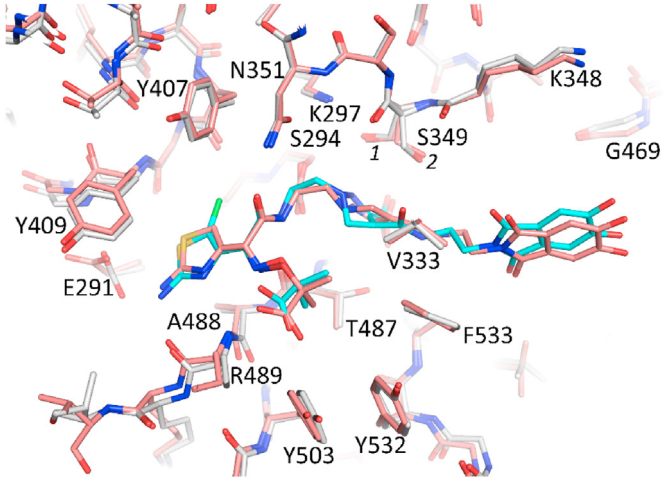

Fig. 7. Superpositioning of the **1** and **2** bound structures of *P. aeruginosa* PBP3. The carbon atoms of the **1**:PBP3 complex is shown in salmon color; while **2** is colored cyan with its protein shown in white.

Table 4
Individual plasma concentrations of **2** after sc (50 mg/kg) dosing in mice, each value represents an individual mouse, showing mean blood levels >1 μg/mL at the 8-h time point.

Time (h)	Sample Conc (ng/ml)			Mean (ng/ml)	SD (ng/ml)
0.167	48690	48689	44921	47433	2176
0.5	20245	14355	14094	16231	3478
1	3138	3515	3186	3280	205
2	3273	2876	3072	3074	199
4	1534	1732	739	1751	526
6	1426	1102	1425	1318	187
8	1001	1473	1126	1200	245
24	678	545	579	601	69

As might have been predicted by the pharmacokinetic results, **1** was not found to have efficacy in the animal model against this carbapenem-resistant strain even though the MIC values indicated the strain had good susceptibility of 0.25 μg/mL (Fig. 9). Importantly, **2**, with superior pharmacokinetics does show a dose-dependent reduction in CFU values against this difficult to treat *P. aeruginosa* strain. It is notable that the MIC value for **2** of 0.5 μg/mL is below the expected blood levels of **2** at the 6 h dosing interval and, in spite of the high protein binding of 94%, encouraging activity was seen (Fig. 9).

2.6. Resistance

Although **2** showed broad coverage against a large panel of resistant clinical isolates of *Acinetobacter* spp. including carbapenem-resistant *A. baumannii*, a fraction of all tested strains (24 of 198, 12%) and the carbapenem-resistant subgroup (15 of 98, 15%) demonstrated MICs ≥16 μg/mL.

Understanding the mechanism or mechanisms of resistance for **2** is important as it allows the optimization of partner agents or alternative dosing schedules to ameliorate potential issues. This knowledge will help predict whether further strains will be susceptible and influence future clinical use, as well as design and synthesis of subsequent analogs.

There are a number of mechanisms that have been identified for resistance to antibiotics for *Acinetobacter* spp. as well as other Gram-negative pathogens. They fall into 4 general categories: 1) degradation of the antibiotic (e.g., β-lactamase hydrolysis); 2) target modification (e.g., PBP mutations or changes in the expression of PBP genes); 3) efflux of the antibiotic from the periplasm or cytoplasm (e.g., mutations or decreased changes in expression of pump genes such as ErmAB-TolC, macA, UadeA-H, mdtABC); or 4) decreased permeability of the bacterial outer membrane (e.g., TolC, OmpH, OPRD genes). All of these represent potential mechanisms for resistance to **2**. Additionally, due to the incorporation of the siderophore moiety as a key component of the antibiotic molecule, changes in the expression of genes related to the bacterial iron transport system could also have an effect on antibiotic susceptibility as was identified as a potential resistance mechanism for cefiderocol, **9** [Ito, A. et al. IDWeek 2018 poster 696. https://idsa.confex.com/idsa/2018/webprogram/Paper69661.html].

2.7. Genomic analysis for resistance genes

Our initial investigation to determine the mechanism of resistance toward **2** seen in *Acinetobacter* spp., as well as *P. aeruginosa* and *K. pneumoniae*, was undertaken by comparing the genomes of susceptible and resistant organisms. Using whole-genome sequencing (WGS), potential resistance genes including β-lactamases, efflux pumps, porin proteins, PBPs, and iron transport were analyzed for potential gene mutations [41] (see supplemental genomic analysis data for details). There were no identified trends in the presence of resistance genes related to β-lactamases, efflux pumps, outer membrane porins, or iron transport when comparing isolates of all analyzed species. When analyzing the PBP genes of *P. aeruginosa*, a mutation in the PBP3, F533L, previously identified as a gain of function mutation for β-lactam antibiotics [42,43] may be partially responsible for resistance to **1** and **2** (Table 5). The side

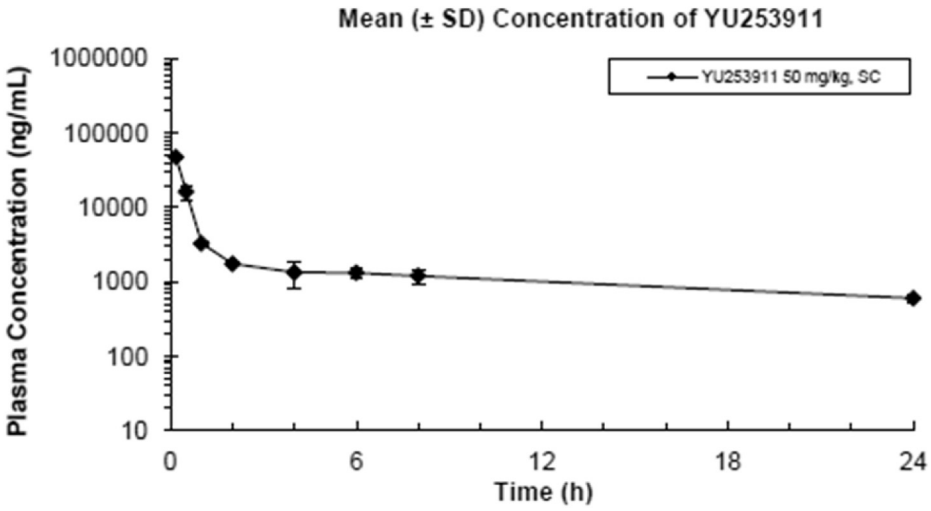

Fig. 8. The mean plasma concentration-time profile for YU253911, **2**, after sc dosing (50 mg/kg) in mice.

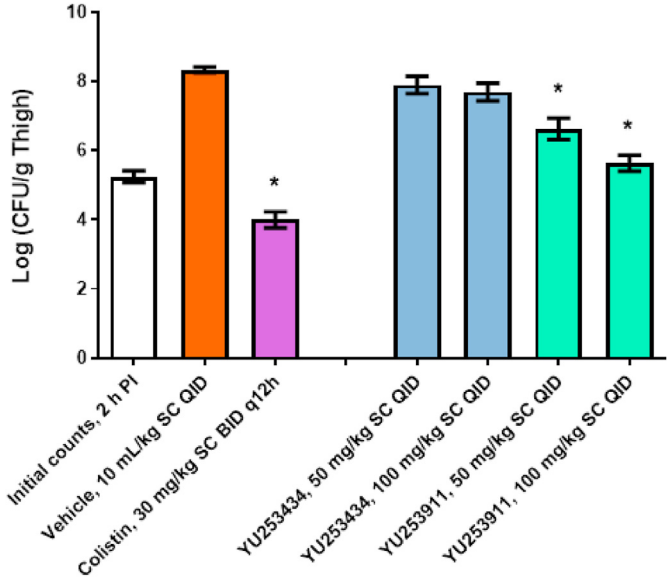

Fig. 9. The test compounds YU253434 **1**, YU253911 **2,** and colistin efficacy in the *P. aeruginosa* AR-BANK#0229 thigh infection model.
(*) A significant difference ($p < 0.05$) between the vehicle control and treatment group was determined by one-way ANOVA followed by Dunnett's test.
Error bars are SEM values.

chain of F533 in the active site of *P. aeruginosa* PBP3 makes contacts with the γ-lactam acylation product as seen in the X-ray structure (Fig. 6).

2.8. β-Lactamase stability

As was previously reported, the dihydroxyphthalimide siderophore mimetic side chain appended to the γ-lactam core was: a) intended to impart stability against β-lactamase hydrolysis; and b) promote periplasm uptake. Thus, γ-Lactam **2** was evaluated as a potential substrate against representative members of all 4 Ambler classes of β-lactamases. We did not observe measurable reactions with KPC-2 (class A *K. pneumoniae* carbapenemase), ADC-7 (class C *Acinetobacter*-derived cephalosporinase) or OXA-23 (class D oxacillinase) when tested as purified isolated enzymes. Class B metallo β-lactamases NDM-1, VIM-2, and IMP-1, however, did demonstrate measurable activity (Table 6). Remarkably, the calculated catalytic efficiencies, k_{cat}/K_m of 0.003–0.02 $\mu M^{-1}s^{-1}$ were orders of magnitude lower than those previously determined for a comparator antibiotic (imipenem 2.7–6.7 $\mu M^{-1}s^{-1}$) [22] and similar to what was previously reported for γ-lactam **1** (0.02–0.07 $\mu M^{-1}s^{-1}$) [22]. Furthermore, the observed stability to purified β-lactamase enzymes correlates with the MIC data, where a relationship was not noted between microbiologic activity and the presence or absence of any β-lactamase gene. See Supplemental Table 3, page 27, for the full listing of the *Acinetobacter* spp. β-lactamase genes in this experiment.

2.9. Efflux inhibitor experiments

To further investigate potential resistance mechanisms, the growth inhibition of **2** in combination with efflux pump inhibitors (EPIs) was examined. The MIC (μg/mL) values of **2** in combination

Table 5
MICs (μg/mL) of γ-lactams **1** and **2** against representative susceptible (MIC ≤4 μg/mL) and resistant (MIC ≥16 μg/mL) clinical isolates of *P. aeruginosa* that have been whole genome sequenced and the identity of the amino acid at position 533: phenylalanine (wild-type) or leucine (mutation shown previously to provide gain of function for β-lactam antibiotics in some resistant strains of *P. aeruginosa*).

P. aeruginosa ID no.	1	2	Position 533 residue
PR-545	≤ 0.25	0.5	Phenylalanine
PR-548	≤ 0.25	1	Phenylalanine
PR-567	≤ 0.25	≤ 0.25	Phenylalanine
PR-672	≤ 0.25	≤ 0.25	Phenylalanine
PR-604	≤ 0.25	≤ 0.25	Phenylalanine
PR-638	>16	0.5	Phenylalanine
PR-676	16	2	Phenylalanine
PR-503	16	16	Phenylalanine
PR-564	>16	>16	Leucine
PR-606	16	>16	Phenylalanine
PR-627	>16	>16	Leucine
PR-635	16	16	Phenylalanine
PR-636	>16	>16	Leucine
PR-651	>16	>16	Leucine
PR-668	>16	>16	Leucine
PR-673	>16	>16	Leucine
PR-677	16	16	Phenylalanine
PR-680	>16	>16	Leucine
PR-688	>16	>16	Leucine
PR-699	>16	>16	Phenylalanine

Table 6
Susceptibility of **2** to β-Lactamase hydrolysis[a].

Metallo-β-lactamase	k_{cat} (s^{-1})	K_m (μM)	k_{cat}/K_m ($\mu M^{-1}s^{-1}$)
NDM-1	35 ± 4	1808 ± 200	0.020 ± 0.002
VIM-2	54 ± 6	4400 ± 450	0.012 ± 0.001
IMP-1	5 ± 1	1490 ± 300	0.003 ± 0.001
KPC-2	NM	NM	NM
ADC-7	NM	NM	NM
OXA-23	NM	NM	NM

[a] Steady-state reactions of **2** were monitored using purified enzymes: KPC-2, ADC-7, OXA-23, NDM-1, VIM-2, and IMP-1. Kinetic parameters provided were determined from double reciprocal plots (Supplemental Figure 2, page 44). Measurable reaction was not detected for KPC-2, ADC-7, or OXA-23 using 200 nM enzyme concentration and 100 μM **2**. NM = not measureable.

with the EPIs carbonyl cyanide 3-chlorophenylhydrazone (CCCP) or phenylalanine-arginine β-naphthylamide (PaβN) were tested against a subgroup of *Acinetobacter* spp. isolates resistant to **2** (Supplemental Table 4, page 32). The EPIs were kept at a constant concentration at levels commonly used in published reports against Gram-negative bacteria (2 μg/mL for CCCP and 32 μg/mL for PAβN). No significant inhibition effect on growth was observed directly from the EPIs, and no consistent effect on MIC values were observed when combined with **2**. Potential synergistic effects were observed for only one isolate, PR-452, when combined with CCCP and since this was not a general effect, a detailed investigation was not pursued.

3. Conclusions

In conclusion, we demonstrate the potency and effectiveness of a novel γ-lactam siderophore antibiotic. Our intent was to build upon previous investigations performed with compound **1**. We show potency against MDR strains of *K. pneumoniae*, *Acinetobacter* spp., and *P. aeruginosa* ($MIC_{50} \leq 0.5$ μg/ml vs. > 8 for meropenem). Consistent with these microbiological findings, molecular analyses reveal stability against problematic β-lactamases. The atomic structure of *P. aeruginosa* PBP-3 at 2.0 Å resolution revealed an important "C-Cl ⋯ O″ interaction with the carbonyl oxygen of Y407. PK/PD and animal testing established that reductions in CFU were significant when compared to colistin. Importantly, toxicity was not evident in a series of assays. Against CRAB, we lowered MICs significantly by combining **2** with sulbactam, designing a novel γ-lactam BLI combination. Studies are planned to further increase our understanding regarding optimal structure activity relationships (SARs) and dosing to overcome resistant infection.

4. Experimental

4.1. Syntheses

The reagents and solvents used for synthesis were of reagent grade quality. Dry solvents were purchased and used as such. All compounds were individually purified by chromatography on silica gel or by recrystallization and were of >95% purity for characterization purposes as determined by LCMS using UV absorption at 220 or 280 nM and/or NMR integration. In practice, compounds were not always purified to >95% purity prior to using in the next synthetic step, and often crude material was of sufficient purity and was carried forward. Copies of the spectra of **2** are included in the Supplemental Information, page 8.

4.1.1. Synthesis of (S,Z)-6-(2-(((1-(tert-butoxy)-2-methyl-1-oxopropan-2-yl)oxy)imino)-2-(5-chloro-2-(tritylamino)thiazol-4-yl)acetamido)-2-((2-(5,6-dihydroxy-1,3-dioxoisoindolin-2-yl)ethyl)carbamoyl)-5-oxo-6,7-dihydro-1H,5H-pyrazolo[1,2-a]pyrazole-3-carboxylic acid

(Z)-2-(((1-(*tert*-butoxy)-2-methyl-1-oxopropan-2-yl)oxy)imino)-2-(5-chloro-2-(tritylamino)thiazol-4-yl)acetic acid [44] **15** (537 mg, 0.89 mmol) in dry dichloromethane (7 mL) and catalytic DMF was cooled in an ice bath and treated with oxalyl chloride (484 μL of 2.0 M solution, 0.97 mmol) and stirred for 1 h. In a second flask starting amine **14** as the TFA salt (348 mg, 0.81 mmol) in dichloromethane (7 mL) was cooled in an ice bath and MSTFA (600 μL, 3.2 mmol) and Hunig's base (773 μL, 4.4 mmol) was added. After stirring for 20 min all of the starting amine was in solution. During this time the dichloromethane from the acid chloride forming reaction was evaporated and placed on a high vacuum to give a colorless foam. This foam was dissolved in dry DCM (7 mL) and added to the MSTFA treated amine followed by the addition of Hunig's base (250 μL, 1.4 mmol). The reaction was allowed to warm to room temperature over 1 h and stirred overnight to give the crude product (S,Z)-6-(2-(((1-(*tert*-butoxy)-2-methyl-1-oxopropan-2-yl)oxy)imino)-2-(2-(tritylamino)thiazol-4-yl)acetamido)-2-((2-(5,6-dihydroxy-1,3-dioxoisoindolin-2-yl)ethyl)carbamoyl)-5-oxo-6,7-dihydro-1H,5H-pyrazolo [1,2-*a*]pyrazole-3-carboxylic acid that was not isolated but directly deprotected in situ.

4.1.2. Synthesis of (S,Z)-6-(2-(2-amino-5-chlorothiazol-4-yl)-2-(((2-carboxypropan-2-yl)oxy)imino)acetamido)-2-((2-(5,6-dihydroxy-1,3-dioxoisoindolin-2-yl)ethyl)carbamoyl)-5-oxo-6,7-dihydro-1H,5H-pyrazolo[1,2-a]pyrazole-3-carboxylic acid (2)

To the crude material from the overnight reaction above (0.82 g, 0.81 mmol) was added triethyl silane (0.64 mL, 4.0 mmol). The solution was cooled in and ice bath and trifluoroacetic acid (6.2 mL, 81 mmol) was added. The ice bath was removed after 30 min and the reaction was stirred at room temperature for 1 h. Toluene (25 mL) was added and the reaction was evaporated to dryness. The crude reaction mixture was dissolved in dimethyl sulfoxide, diluted with water and chromatographed using reverse phase C18 MPLC eluting with 0–40% acetonitrile with 0.1% formic acid in water with 0.1% formic acid to give the product (S,Z)-6-(2-(2-amino-5-chlorothiazol-4-yl)-2-(((2-carboxypropan-2-yl)oxy)imino)acetamido)-2-((2-(5,6-dihydroxy-1,3-dioxoisoindolin-2-yl)ethyl)carbamoyl)-5-oxo-6,7-dihydro-1H,5H-pyrazolo [1,2-*a*]pyrazole-3-carboxylic acid, **2**, as a yellow powder after lyophilization (139 mg, 23%). ^{1}H NMR (400 MHz, DMSO-d_6) δ 12.61 (s, 1H), 10.34 (s, 4H), 8.78 (d, J = 8.34 Hz, 1H), 8.56–7.91 (m, 1H), 7.38 (s, 2H), 7.12 (s, 4H), 5.03 (dt, J = 8.05, 10.89 Hz, 1H), 4.11 (d, J = 12.50 Hz, 1H), 3.81 (dd, J = 6.81, 10.26 Hz, 2H), 3.67–3.48 (m, 2H), 2.96 (dd, J = 8.71, 10.98 Hz, 1H), 1.66–1.36 (m, 6H). Mass spectrum $M+H^+$ = 721.0; HRMS (ESI/QTOF) Calcd for $C_{27}H_{25}Cl_1N_8O_{12}S_1$ 720.1001, found $M+H^+$ 721.1077.

4.2. Minimum inhibitory concentrations, MICs

Bacterial strains used were from previously described collections [22,45]. MICs were determined using the general recommendations of the Clinical and Laboratory Standards Institute (CLSI). Standard broth microdilution methods were followed but with a slightly lower inoculum (6×10^4 cfu/mL) which afforded no difference in MICs in our testing. MICs were performed using iron-depleted cation-adjusted Mueller-Hinton broth, except as mentioned elsewhere, using a standard protocol used with other siderophore-containing antibiotics.

4.3. Protein expression, purification, crystallization, and structure determination of the compound 2 P. aeruginosa PBP3 complex

The *P. aeruginosa* PBP3 protein was expressed, purified, and crystallized as previously described [22]. A crystal of *P. aeruginosa* PBP3 was soaked with 2 mM compound **2** for 43 h in mother liquor before freezing the crystal in liquid nitrogen prior to data collection. Data were collected at the SSRL synchrotron beamline 12-2 and processed to 2.0 Å resolution using HKL3000 [46]. The structure was solved using molecular replacement using PHASER [47] with the PBP3 ceftazidime complex protein coordinates as the search model (PBD ID 3PBO). The structure was refined using REFMAC 5 [48], and the program Coot [49] was used for model building. Refinement parameter files for compound **2** were generated using ACEDRG [50]. Molecular figures were generated using Pymol (www.pymol.org). The coordinates and structure factors of the *P. aeruginosa* PBP3 YU253911 complex have been deposited with the Protein Data Bank (PDB ID 7LC4).

4.4. PBP binding kinetics

A method was adapted from the work using purified, soluble *P. aeruginosa* PBP3 and Bocillin™, a fluorescent β-lactam and substrate [37]. Reactions were conducted in 10 mM phosphate-buffered saline at pH 7.4 using 1.6 μM *P. aeruginosa* PBP3 incubated with increasing concentrations of **2**. To ensure that equilibrium between **2** and PBP3 occurred, the enzyme was preincubated with the compound for 20 min at 37 °C before the addition of 50 μM Bocillin™ and then incubated for an additional 20 min. The reactions were stopped by adding SDS-PAGE loading dye and boiling for 2 min. Samples were analyzed by SDS-PAGE and the gel illuminated at λ = 365 nm and imaged with a Fotodyne gel imaging system. ImageJ analysis software was used to assign fluorescence intensity (FI). The IC_{50} was calculated as the concentration of **2** required to reduce the FI of the Bocillin™-labeled protein by 50%.

4.5. β-lactamase stability testing

Steady-state kinetics were determined with purified enzymes (KPC-2, ADC-7, OXA-23, NDM-1, VIM-2, and IMP-1) using an Agilent model 8453 diode array spectrophotometer as previously described [22]. Assays were performed at 25 °C (room temperature) using 10 mM PBS, pH 7.4 (KPC-2, ADC-7), 50 mM sodium phosphate buffer supplemented with 20 mM sodium bicarbonate (OXA-23) or 10 mM HEPES, pH 7.5, 0.2 M NaCl, 50 μg/ml bovine serum albumin, and 50 μM Zn (NDM-1, VIM-2, and IMP-1).

Compound **2** was used as a substrate at excess molar concentrations to establish pseudo-first-order kinetics. The following extinction coefficient was used: **2**, $\Delta\epsilon 336 = -4362\ M^{-1}\ cm^{-1}$. For velocity determinations, a 0.2 cm path length quartz cuvette was employed. Hydrolysis of 600 μM **2** was monitored over time until completion. Based on the starting absorbance (λ = 336 nm, 600 μM **2**) and final absorbance (λ = 336 nm, 0 μM **2**), concentrations of **2** were determined along the progress curve and velocities during a 10 s period for each concentration calculated. A double reciprocal plot (1/[S] vs. 1/*V*) was employed to obtain the steady-state kinetic parameters V_{max}, k_{cat}, and K_m according to Equations (1) and (2):

$$1/V = K_m/V_{max}(1/[S]) + 1/V_{max} \quad \text{Eq. 1}$$

$$k_{cat} = V_{max}/[E] \quad \text{Eq. 2}$$

where V = reaction velocity, K_m = Michaelis-Menten constant, V_{max} = maximum reaction velocity, and [S] = substrate concentration. Compound **1** was retested with NDM-1, VIM-2, and IMP-1 using this same method, resulting in similar values to those previously reported [22] (Supplemental Figure 1, page 43 and Supplemental Table 5, page 44).

4.6. Genomic analysis

Acinetobacter spp., and *K. pneumoniae* sequences were downloaded from the sequencing read archive project PRJNA384060, PRJNA384065, and PRJNA339843, respectively (National Center for Biotechnology Information, U.S. National Library of Medicine, 8600 Rockville Pike, Bethesda MD, 20894 USA). *Pseudomonas aeruginosa* were sequenced by the Illumina Hiseq platform with 2x150bp paired-end sequencing. Reads were assembled and annotated using PATRIC, the Pathosystems Resource Integration Center [41]. Antibiotic resistant genes were identified using RES Finder (Center for Genomic Epidemiology; http://www.genomicepidemiology.org/). Amino acid variations were identified by comparison of strains to the *Acinetobacter* ATCC 17978 *and* ATCC 19606, *Pseudomonas aeruginosa* PA01, or *Klebsiella pneumoniae* MGH 78578 (GenBank Accessions CP000523, ACQB00000000, CP001183, CP000647).

Accession codes

PDB code for *P. aeruginosa* PBP3 with bound YU253911, **2,** is PDB ID 7LC4. Authors will release the atomic coordinates upon article publication.

Declaration of competing interest

The authors declare that they have no known competing financial interests or personal relationships that could have appeared to influence the work reported in this paper.

Acknowledgements

MSP: Financial support was provided by the Program in Innovative Therapeutics for Connecticut's Health grant by the Connecticut Bioscience Innovation Fund, administered by the Connecticut Innovations. RAB: Research reported in this publication was supported by the National Institute of Allergy and Infectious Diseases of the National Institutes of Health (NIH) under Award Numbers R01AI100560, R01AI063517, and R01AI072219. This study was also supported in part by funds and/or facilities provided by the Cleveland Department of Veterans Affairs, Award Numbers 1I01BX002872 to KMP-W and 1I01BX001974 to RAB, from the Biomedical Laboratory Research & Development Service of the VA Office of Research and Development, and the Geriatric Research Education and Clinical Center VISN 10 (RAB). The content is solely the responsibility of the authors and does not necessarily represent the official views of the NIH or the Department of Veterans Affairs.

BNK: Research reported in this publication was supported by a grant from the National Institutes of Health, R01AI090155.

RAB wishes to gratefully thank the Antimicrobial Resistance Leadership Group (ARLG) for the use of the isolates. The research described in this publication is supported, at least in part, by a grant from the National Institutes of Health through Duke University and the findings, opinions, and recommendations expressed herein are those of the authors and not necessarily those of Duke University or the National Institutes of Health. This study is also supported by the National Institute of Allergy and Infectious Diseases of the National Institutes of Health (NIH) under Award Number UM1AI104681. This work utilized NIAID's suite of preclinical services for *in vitro* and *in vivo* assessments (Contract Nos. 75N93019D00022/75N93020F00001 and HHSN272201700020I/75N93020F00159).

FVDA: We also thank Stanford Synchrotron Radiation Lightsource (SSRL) for help with data collection. Use of the SSRL, SLAC National Accelerator Laboratory, is supported by the U.S. Department of Energy, Office of Science, Office of Basic Energy Sciences under Contract No. DE-AC02-76SF00515. The SSRL Structural Molecular Biology Program is supported by the DOE Office of Biological and Environmental Research, and by the National Institutes of Health, National Institute of General Medical Sciences (including P41GM103393). The contents of this publication are solely the responsibility of the authors and do not necessarily represent the official views of NIGMS or NIH.

Appendix A. Supplementary data

Supplementary data to this article can be found online at https://doi.org/10.1016/j.ejmech.2021.113436.

References

[1] a) Centers for Disease Control and Prevention, Antibiotic resistance threats in the United States, 2019 AR threats report. https://www.cdc.gov/drugresistance/biggest-threats.html, 2019. (Accessed 11 March 2020);
b) A. Cassini, L.D. Högberg, D. Plachouras, A. Quattrocchi, A. Hoxha, G.S. Simonsen, M. Colomb-Cotinat, M.E. Kretzschmar, B. Devleesschauwer, M. Cecchini, D.A. Ouakrim, T.C. Oliveira, M.J. Struelens, C. Suetens, D.L. Monnet, And the Burden of AMR Collaborative Group; Attributable deaths and disability-adjusted life-years caused by infections with antibiotic-resistant bacteria in the EU and the European Economic Area in 2015: a population-level modelling analysis, Lancet Infect. Dis. 19 (2019) 56–66, https://doi.org/10.1016/S1473-3099(18)30605-4.

[2] World Health Organization, Antimicrobial resistance: global report on surveillance. https://www.who.int/antimicrobial-resistance/publications/surveillancereport/en/, 2014. (Accessed 11 March 2020).

[3] B. Spellberg, R. Guidos, D. Gilbert, J. Bradley, H.W. Boucher, W.M. Scheld, J.G. Bartlett, J. Edwards Jr., Infectious Diseases Society of America, the epidemic of antibiotic-resistant infections: a call to action for the medical community from the Infectious Diseases Society of America, Clin. Infect. Dis. 46 (2008) 155–164, https://doi.org/10.1086/524891.

[4] H.W. Boucher, G.H. Talbot, J.S. Bradley, J.E. Edwards, D. Gilbert, L.B. Rice, M. Scheld, B. Spellberg, J. Bartlett, Bad bugs, no drugs: no ESKAPE! an update from the Infectious Diseases Society of America, Clin. Infect. Dis. 48 (2009) 1–12, https://doi.org/10.1086/'5955011.

[5] World Health Organization, Global priority list of antibiotic-resistant bacteria to guide research, discovery, and development of new antibiotics. https://www.who.int/medicines/publications/global-priority-list-antibiotic-resistant-bacteria/en/, 2017. (Accessed 11 March 2020).

[6] A.Y. Peleg, D.C. Hooper, Hospital-acquired infections due to Gram-negative bacteria, N. Engl. J. Med. 362 (2010) 1804–1813, https://doi.org/10.1056/NEJMra0904124.

[7] E.R. Sydnor, T.M. Perl, Hospital epidemiology and infection control in acute-care settings, Clin. Microbiol. Rev. 24 (2011) 141–173, https://doi.org/10.1128/CMR.00027-10.

[8] M. Hassani, The crisis of Gram-negative bacterial resistance: is there any hope for ESKAPE? Clin. Res. Infect. Dis. 1 (2014) 1005–1009.

[9] L.L. Silver, Challenges of antibacterial discovery, Clin. Microbiol. Rev. 24 (2011) 71–109, https://doi.org/10.1128/CMR.00030-10.

[10] D.J. Payne, M.N. Gwynn, D.J. Holmes, D.L. Pompliano, Drugs for bad bugs: confronting the challenges of antibacterial discovery, Nat. Rev. Drug Discov. 6 (2007) 29–40, https://doi.org/10.1038/nrd2201.

[11] A.D. So, N. Gupta, S.K. Brahmachari, I. Chopra, B. Munos, C. Nathan, K. Outterson, J.P. Paccaud, D.J. Payne, R.W. Peeling, M. Spigelman, J. Weigelt, Towards new business models for R&D for novel antibiotics, Drug Resist. Updates 14 (2011) 88–94, https://doi.org/10.1016/j.drup.2011.01.006.

[12] D.M. Livermore, Multiple mechanisms of antimicrobial resistance in *Pseudomonas aeruginosa*: our worst nightmare? Clin. Infect. Dis. 34 (2002) 634–640, https://doi.org/10.1086/338782.

[13] M. Tomas, M. Doumith, M. Warner, J.F. Turton, A. Beceiro, G. Bou, D.M. Livermore, N. Woodford, Efflux pumps, OprD porin, AmpC beta-lactamase, and multiresistance in *Pseudomonas aeruginosa* isolates from cystic fibrosis patients, Antimicrob. Agents Chemother. 54 (2010) 2219–2224, https://doi.org/10.1128/AAC.00816-09.

[14] R.J. Ternansky, S.E. Draheim, [4.3.0] Pyrazolidionones as potential antibacterial agents, Tetrahedron Lett. 29 (1988) 6569–6572.

[15] N.E. Allen, J.N. Hobbs Jr., D.A. Preston, J.R. Turner, C.Y. Wu, Antibacterial properties of the bicyclic pyrazolidinones, J. Antibiot. (Tokyo) 43 (1990) 92–99, https://doi.org/10.7164/antibiotics.43.92.

[16] R.J. Ternansky, S.E. Draheim, Structure-activity relationship within a series of pyrazolidinone antibacterial agents. 1. Effect of nuclear modification on in vitro activity, J. Med. Chem. 36 (1993) 3219–3223, https://doi.org/10.1021/jm00074a001.

[17] R.J. Ternansky, S.E. Draheim, A.J. Pike, F.T. Counter, J.A. Eudaly, J.S. Kasher, Structure-activity relationship within a series of pyrazolidinone antibacterial agents. 2 Effect of side-chain modification on in vitro activity and pharmacokinetic parameters, J. Med. Chem. 36 (1993) 3224–3229, https://doi.org/10.1021/jm00074a002.

[18] D.B. Boyd, Application of the hypersurface iterative projection method to bicyclic pyrazolidinone antibacterial agents, J. Med. Chem. 36 (1993) 1443–1449, https://doi.org/10.1021/jm00062a017.

[19] L.N. Jungheim, S.K. Sigmund, J.W. Fisher, Bicyclic pyrazolidinones, a new class of antibacterial agents based on the β-lactam model, Tetrahedron Lett. 28 (1987) 285–288.

[20] L.N. Jungheim, S.K. Sigmund, N.D. Jones, J. Swartzendruber, Bicyclic pyrazolidinones, steric and electronic effects on antibacterial activity, Tetrahedron Lett. 28 (1987) 289–292.

[21] L.N. Jungheim, L. N, R.J. Ternansky, R.E. Holmes, Bicyclic Pyrazolidinone Antibacterial Agents Drugs of the Future 15 (1990) 149, https://doi.org/10.1358/dof.1990.015.02.114554.

[22] J.A. Goldberg, H. Nguyen, V. Kumar, E.J. Spencer, D. Hoyer, E.K. Marshall, A. Cmolik, M. O'Shea, S.H. Marshall, A.M. Hujer, K.M. Hujer, S.D. Rudin, T.N. Domitrovic, C.R. Bethel, K.M. Papp-Wallace, L.K. Logan, F. Perez, M.R. Jacobs, D. van Duin, B.M. Kreiswirth, R.A. Bonomo, M.S. Plummer, F. van den Akker, A γ-lactam siderophore antibiotic effective against multidrug-resistant gram-negative, Bacilli J. Med. Chem. 63 (11) (2020) 5990–6002, https://doi.org/10.1021/acs.jmedchem.0c00255.

[23] P. Cornelis, S. Matthijs, L. Van Oeffelen, Iron uptake regulation in *Pseudomonas aeruginosa*, Biometals 22 (2009) 15–22, https://doi.org/10.1007/s10534-008-9193-0.

[24] a) B.R. Wilson, A.R. Bogdan, M. Miyazawa, K. Hashimoto, Y. Tsuji, Siderophores in Iron Metabolism: from Mechanism to Therapy Potential Trends in Molecular Medicine, vol. 22, 2016, pp. 1077–1090, 12;
b) I.J. Schalk, G.L.A. Mislin, Bacterial iron uptake pathways: gates for the import of bactericide compounds, J. Med. Chem. 60 (2017) 4573–4576, https://doi.org/10.1021/acs.jmedchem.7b00554.

[25] A. Luscher, l. Moynie, P.S. Auguste, D. Bumann, L. Mazza, d. Pletzer, J.H. Naismith, T. Kohler, TonB-Dependant receptor repertoire of *Pseudomonas aeruginosa* for uptake of siderophore-drug conjugates, *Antimicrob. Agents* Chemother. 63 (6) (2018), https://doi.org/10.1128/AAC.00097-18 e00097–e00118.

[26] M.G. Baudart, L.F. Hennequin, Synthesis and biological activity of C-3' ortho dihydroxyphthalimido cephalosporins, J. Antibiot. 46 (9) (1993) 1458–1470, https://doi.org/10.7164/antibiotics.46.1458.

[27] S.R. Evans, T.T.T. Tran, A.M. Hujer, C.B. Hill, K.M. Hujer, J.R. Mediavilla, C. Manca, T.N. Domitrovic, F. Perez, M. Farmer, K.M. Pitzer, B.M. Wilson, B.N. Kreiswirth, R. Patel, M.R. Jacobs, L. Chem, V.G. Fowler, H.F. Chambers, R.A. Bonomo, Rapid molecular diagnostics to inform empiric use of Ceftazidime/Avibactam and Ceftolozane/Tazobactam against *Pseudomonas aeruginosa*: primers IV, Clin. Infect. Dis. 68 (2019) 1823–1830, https://doi.org/10.1093/cid/ciy801.

[28] O. Henig, E. Cober, S.S. Richter, F. Perez, R.A. Salata, R.C. Kalayjian, R.R. Watkins, S. Marshall, S.D. Rudin, T.N. Domitrovic, A.M. Hujer, K.M. Hujer, Y. Doi, S. Evans, V.G. Fowler Jr., R.A. Bonomo, D. van Duin, K.S. Kaye, A prospective observational study of the epidemiology, management, and outcomes of skin and soft tissue infections due to carbapenem-resistant Enterobacteriaceae, Open Forum Infect Dis 4 (2017) ofx157, https://doi.org/10.1093/ofid/ofx157.

[29] A. Ito, T. Nishikawa, S. Matsumoto, H. Yoshizawa, T. Sato, R. Nakamura, M. Tsuji, Y. Yamano, Siderophore cephalosporin Cefiderocol utilizes ferric iron transporter systems for antibacterial activity against *Pseudomonas aeruginosa*, Antimicrob. Agents Chemother. 60 (2016) 7396–7401, https://doi.org/10.1128/AAC.01405-16.

[30] S.R. Evans, A.M. Hujer, H. Jiang, C.B. Hill, K.M. Hujer, J.R. Mediavilla, C. Manca, T.T Tran, T.N. Domitrovic, P.G. Higgins, H. Seifert, B.N. Kreiswirth, R. Patel, M.R. Jacobs, L. Chen, R. Sampath, T. Hall, C. Marzan, V.G. Fowler, H.F. Chambers, R.A. Bonomo, Antibacterial Resistance Leadership Group. Informing antibiotic treatment decisions: evaluating rapid molecular diagnostics to identify susceptibility and resistance to carbapenems against *Acinetobacter* spp. in PRIMERS III, J. Clin. Microbiol. 55 (2017) 134–144, https://doi.org/10.1128/JCM.01524-16.

[31] M. Nechifor, D. Buic, E. Diaconu, A. Poiata, E. Teslariu, C. Filip, A. Negru, C. Antonescu, Pharmacological studies of sulbactam and its association with semisynthetic beta-lactam antibiotics, Rev. Med.-Chir. Soc. Med. Nat. Iasi 96 (1992) 51–55.

[32] V.V. Berezhinskaia, G.V. Dolgova, G.G. Egorenko, T.P. Svinogeeva, L.A. Shtegel'man, T.V. Smolkina, A.V. Nikitin, Study of general toxic and organotropic properties of ampicillin combined with sulbactam, Antibiot. Khimioter. 37 (1992) 25–28, https://doi.org/10.1517/17425250903145251.

[33] A.P. Betrosian, E.E. Douzinas, Ampicillin-sulbactam: an update on the use of parenteral and oral forms in bacterial infections, Expet Opin. Drug Metabol. Toxicol. 5 (2009) 1099–1112.

[34] J.M. Benson, M.C. Nahata, Sulbactam/ampicillin, a new beta-lactamase inhibitor/beta-lactam antibiotic combination, Drug Intell. Clin. Pharm. 22 (1988) 534–541, https://doi.org/10.1177/106002808802200702.

[35] B. Hampel, H. Lode, G. Bruckner, P. Koeppe, Comparative pharmokinetics of sulbactam/ampicillin and clavulanic acid/amoxycillin in human volunteers,

Drugs 35 (1988) 29–33, https://doi.org/10.2165/00003495-198800357-00007.
[36] W.F. Penwell, A.B. Shapiro, R.A. Giacobbe, R.F. Gu, N. Gao, J. Thresher, R.E. McLaughlin, M.D. Huband, B.L.M. DeJonge, D.E. Ehmann, A.A. Miller, Molecular mechanisms of sulbactam antibacterial activity and resistance determinants in *Acinetobacter baumannii*, Antimicrob. Agents Chemother. 59 (2015) 1680–1689, https://doi.org/10.1128/AAC.04808-14.
[37] K.M. Papp-Wallace, B. Senkfor, J. Gatta, W. Chai, M.A. Taracila, V. Shanmugasundaram, S. Han, R.P. Zaniewski, B.M. Lacey, A.P. Tomaras, M.J. Skalweit, M.E. Harris, L.B. Rice, J.D. Buynak, R.A. Bonomo, Early insights into the interactions of different β-lactam antibiotics and β-lactamase inhibitors against soluble forms of *Acinetobacter baumannii* PBP1a and *Acinetobacter* sp, PBP3. *Antimicrob. Agents Chemother.* 56 (2012) 5687–5692. Doi: 1128/AAC.01027-12.
[38] I. Polsinelli, M. Savko, C. Rouanet-Mehouas, L. Ciccone, S. Nencetti, E. Orlandini, E.A. Stura, W. Shepard, Comparison of helical scan and standard rotation methods in single-crystal X-ray data collection strategies, J. Synchrotron Radiat. 24 (Pt 1) (2017 Jan 1) 42–52, https://doi.org/10.1107/S1600577516018488.
[39] C. Bissantz, B. Kuhn, M. Stahl, A medicinal chemist's guide to molecular interactions, J. Med. Chem. 53 (14) (2010) 5061–5084, https://doi.org/10.1021/jm100112j.
[40] N.K. Shinda, A.G. de Brevern, P. Schmidtke, Halogens in protein-ligand binding mechanism: a structural perspective, J. Med. Chem. 62 (21) (2019) 9341–9356, https://doi.org/10.1021/acs.jmedchem.8b01453.
[41] J.J. Davis, A.R. Wattam, R.K. Aziz, T. Brettin, R. Butler, R.M. Butler, P. Chlenski, N. Conrad, A. Dickerman, E.M. Dietrich, J.L. Gabbard, S. Gerdes, A. Guard, R.W. Kenyon, D. Machi, C. Mao, D. Murphy-Olson, M. Nguyen, E.K. Nordberg, G.J. Olsen, R.D. Olson, J.C. Overbeek, R. Overbeek, B. Parrello, G.D. Pusch, M. Shukla, C. Thomas, M. VanOeffelen, V. Vonstein, A.S. Warren, F. Xia, D. Xie, H. Yoo, R. Stevens, The PATRIC Bioinformatics Resource Center: expanding data and analysis capabilities, Nucleic Acids Res. 48 (2020) 606–612, https://doi.org/10.1039/nar/gkz943, 4,5.
[42] S. Han, R.P. Zaniewski, E.S. Marr, B.M. Lacey, A.P. Tomaras, A. Evdokimov, R.J. Miller, V. Shanmugasundaram, Structural basis for effectiveness of siderophoreconjugated monocarbams against clinically relevant strains of *Pseudomonas aeruginosa*, Proc. Natl. Acad. Sci. United States Am. 107 (2010) 22002–22007, https://doi.org/10.1073/pnas/1013092107.
[43] C. López-Causapé, G. Cabot, E. del Barrio-Tofiño, A. Oliver, The versatile mutational resistome of *Pseudomonas aeruginosa*, Front. Microbiol. 9 (2018) 1–9, https://doi.org/10.3389/fmicb.2018.00685.
[44] Preparation of Siderophore Conjugated Pyrazolidinones, and Analogs Thereof as Antibacterial Agents; Plummer, M.; Hoyer, D.; Spencer, E.; WO2020018929..
[45] S.R. Evans, A.M. Hujer, H. Jiang, C.B. Hill, K.M. Hujer, J.R. Mediavilla, C. Manca, T.T. Tran, T.N. Domitrovic, P.G. Higgins, H. Seifert, B.N. Kreiswirth, R. Patel, M.R. Jacobs, L. Chen, R. Sampath, T. Hall, C. Marzan, V.G. Fowler Jr., H.F. Chambers, R.A. Bonomo, Informing antibiotic treatment decisions: evaluating rapid molecular diagnostics to identify susceptibility and resistance to carbapenems against *Acinetobacter* spp. in PRIMERS III, J. Clin. Microbiol. 55 (2016) 134–144, https://doi.org/10.1128/JCM.01524-16.
[46] M. Wladek, M. Cymborowski, O. Zbyszek, M. Chruszcz, HKL-3000: the integration of data reduction and structure solution–from diffraction images to an initial model in minutes *Acta*, Crystallogr D Biol Crystallogr 62 (Pt 8) (2006 Aug) 859–866, https://doi.org/10.1107/S0907444906019949.
[47] A.J. McCoy, R.W. Grosse-Kunstleve, P.D. Adams, M.D. Winn, L.C. Storoni, R.J. Read, Phaser crystallographic software, J. Appl. Crystallogr. 40 (2007) 658–674, https://doi.org/10.1107/S0021889807021206.
[48] G.N. Murshudov, P. Skubak, A.A. Lebedev, N.S. Pannu, R.A. Steiner, R.A. Nicholls, M.D. Winn, F. Long, A.A. Vagin, REFMAC5 for the refinement of macromolecular crystal structures, Acta Crystallogr. Sect. D Biol. Crystallogr. 67 (2011) 355–367, https://doi.org/10.1107/S0907444911001314, 2011.
[49] P. Emsley, K.C. Cowtan, COOT: model-building tools for molecular graphics, Acta Crystallogr. Sect. D Biol. Crystallogr. 60 (2004) 2126–2132, https://doi.org/10.1107/S0907444904019158.
[50] F. Long, R.A. Nicholls, P. Emsley, S. Graaeulis, A. Merkys, A. Vaitkus, G.N. Murshudov, AceDRG: a stereochemical description generator for ligands, Acta Crystallogr D Struct Biol 73 (Pt 2) (2017 Feb 1) 112–122, https://doi.org/10.1107/S2059798317000067.